Pure appl. geophys. 158 (2001) 1165–1188
0033–4553/01/071165–24 $ 1.50 + 0.20/0

Pure and Applied Geophysics

Mapping Crustal Heterogeneity Using *Lg* Propagation Efficiency Throughout the Middle East, Mediterranean, Southern Europe and Northern Africa

D. E. McNamara[1] and W. R. Walter[2]

Abstract — In this paper we describe a technique for mapping the lateral variation of *Lg* characteristics such as *Lg* blockage, efficient *Lg* propagation, and regions of very high attenuation in the Middle East, North Africa, Europe and the Mediterranean regions. *Lg* is used in a variety of seismological applications from magnitude estimation to identification of nuclear explosions for monitoring compliance with the Comprehensive Nuclear-Test-Ban Treaty (CTBT). These applications can give significantly biased results if the *Lg* phase is reduced or blocked by discontinuous structure or thin crust. Mapping these structures using quantitative techniques for determining *Lg* amplitude attenuation can break down when the phase is below background noise. In such cases *Lg* blockage and inefficient propagation zones are often mapped out by hand. With our approach, we attempt to visually simplify this information by imaging crustal structure anomalies that significantly diminish the amplitude of *Lg*. The visualization of such anomalies is achieved by defining a grid of cells that covers the entire region of interest. We trace *Lg* rays for each event/station pair, which is simply the great circle path, and attribute to each cell a value equal to the maximum value of the *Lg*/*P-coda* amplitude ratio for all paths traversing that particular cell. The resulting map, from this empirical approach, is easily interpreted in terms of crustal structure and can successfully image small blockage features often missed by analysis of raypaths alone. This map can then be used to screen out events with blocked *Lg* prior to performing *Q* tomography, and to avoid using *Lg*-based methods of event identification for the CTBT in regions where they cannot work.

For this study we applied our technique to one of the most tectonically complex regions on the earth. Nearly 9000 earthquake/station raypaths, traversing the vast region comprised of the Middle East, Mediterranean, Southern Europe and Northern Africa, have been analyzed. We measured the amplitude of *Lg* relative to the *P-coda* and mapped the lateral variation of *Lg* propagation efficiency. With the relatively dense coverage provided by the numerous crossing paths we are able to map out the pattern of crustal heterogeneity that gives rise to the observed character of *Lg* propagation. We observe that the propagation characteristics of *Lg* within the region of interest are very complicated but are readily correlated with the different tectonic environments within the region. For example, clear strong *Lg* arrivals are observed for paths crossing the stable continental interiors of Northern Africa and the Arabian Shield. In contrast, weakened to absent *Lg* is observed for paths crossing much of the Middle East, and *Lg* is absent for paths traversing the Mediterranean. Regions that block *Lg* transmission within the Middle East are very localized and include the Caspian Sea, the Iranian Plateau and the Red Sea. Resolution is variable throughout the region and strongly depends on the distribution of seismicity and recording stations. *Lg*

[1] USGS, Golden, CO, USA.
[2] Lawrence Livermore National Laboratory, Livermore, CA, USA.

Correspondence to: Daniel E. McNamara, USGS, Box 25046, MS 966, Denver, CO 80225, E-mail: mcnamara@ghtmail.cr.usgs.gov

propagation is best resolved within the Middle East where regions of crustal heterogeneity on the order of 100 km are imaged (e.g., South Caspian Sea and Red Sea). Crustal heterogeneity is resolvable but is poorest in seismically quiescent Northern Africa.

Key words: *Lg* regional phase seismology, attenuation, CTBT, nuclear explosion.

Introduction

The seismic phase *Lg* often contains the largest amplitudes in regional continental seismograms and is thus used for many purposes in seismological investigations including, magnitude estimation, source spectra and moment determination, and for discriminating explosions from earthquakes for monitoring the Comprehensive Nuclear-Test-Ban Treaty (CTBT). However, because this phase is strongly influenced by the crustal waveguide it also exhibits extreme variations in its amplitude relative to other seismic phases. Indeed it is well known that the phase can be completely absent from regional seismograms that traverse regions of thin crust (e.g., ZHANG and LAY, 1995) or very strong attenuation. Traditional quantitative amplitude measurement techniques such as attenuation Q estimation or attenuation tomography will fail in cases where *Lg* is completely absent due to the impossibility of measuring the amplitude of a phase that is below the background noise. Such regions, that never show efficient *Lg* propagation, are often mapped out by hand, based on examining all available regional seismograms (e.g., RODGERS *et al.*, 1997). In this paper we apply a more quantitative approach to such mapping by plotting the maximum *Lg* amplitude normalized by the *P-coda* in cells across a region. Our main goal in this paper is to map *Lg* characteristics such as *Lg* blockage, efficient *Lg* propagation, and regions of very high attenuation in a vast area that includes the Middle East, North Africa, Europe and the Mediterranean.

The regional mapping aspect of our work expands upon the previous work of numerous scientists (e.g., KADINSKY-CADE *et al.*, 1981, RODGERS *et al.*, 1997) by presenting a method of graphically representing *Lg* propagation characteristics. Our approach maps empirical observations of *Lg*/*P-coda* amplitude ratios and successfully images alternating regions of efficient, inefficient and absent *Lg* transmission. This is achieved by tracing *Lg* rays through a grid of cells that covers the region of interest. We then attribute to each cell the maximum value of the *Lg*/*P-coda* amplitude ratio for all paths traversing that particular cell. The resulting map successfully images *Lg* propagation characteristics often missed by simple analysis of individual raypaths alone. Our mapping technique is also an expansion of two methods previously presented by CAMPILLO *et al.* (1993) and KENNETT *et al.* (1985). We will briefly describe these previous methods in a later section and demonstrate how our empirical amplitude ratio approach contributes to a better assessment of *Lg* propagation characteristics.

This study has two main goals: To map out crustal heterogeneity as illuminated by *Lg* propagation efficiency and to determine regions of blockage or severe attenuation for CTBT monitoring and as a pre-screen for *Q* tomography.

Crustal structure. We intend to understand how the various geologic crustal structures of this tectonically complex region affect the amplitude of high-frequency (0.5–5 Hz) *Lg* arrivals. *Lg* is commonly thought to be generated by a superposition of higher-mode surface waves (OLIVER and EWING, 1957; EWING *et al*., 1957; KNOPOFF *et al*., 1973; MITCHELL, 1995) or, as its group velocity implies, *Lg* propagates as multiply reflected shear waves trapped within the crust (GUTENBERG, 1955; PRESS and EWING, 1952; HERRIN and RICHMOND, 1960; BOUCHON, 1982). *Lg* is of tectonic and geologic interest because it is commonly observed that lateral crustal heterogeneity plays a significant role in shaping the characteristics of the *Lg* signal (RUZAIKIN *et al*., 1977; KENNETT *et al*., 1985; KENNETT, 1986; MCNAMARA *et al*., 1996; RODGERS *et al*., 1997). Consequently, *Lg* carries information about the average crustal shear-wave velocity and apparent attenuation along its path and is sensitive to varying tectonic environments.

CTBT. A second motivation for this study is that *Lg* plays an important role in event discrimination efforts for the CTBT. It is commonly observed that explosions are less efficient at producing *Lg* than earthquakes and *P*/*Lg* amplitude ratios are often used to discriminate the two event types (e.g., WALTER *et al*., 1995; HARTSE *et al*., 1997). An accurate understanding of the factors that affect the variation of *Lg* amplitude and propagation characteristics is important to enable effective discrimination between naturally occurring earthquakes and nuclear explosions.

Factors Affecting Lg Propagation

For naturally occurring earthquakes, *Lg* is a seismic wavetrain that travels with a group velocity of about 3.5 km/s and is generally the largest amplitude arrival on all three components of motion on regional short-period seismograms. The absence of *Lg* on the regional seismogram can be caused by several factors. First, for small magnitude events, *Lg* amplitude can be well beneath background noise levels. Second, high attenuation (low *Q*) can reduce *Lg* amplitude to below noise levels. It is generally observed that *Lg* attenuation is higher for regions with active tectonism than for stable continental interiors (AKI, 1980a, b; MCNAMARA *et al*., 1996). Third, crustal structure plays an important role in determining the amplitude and propagation of *Lg*. The presence of *Lg* is often used to infer the existence of continental crust because *Lg* quickly loses energy in the thin waveguide provided by oceanic crust (KENNETT, 1986; ZHANG and LAY, 1995). Also, *Lg* propagation is affected by variations of the crustal waveguide along its path due to scattering along faults and fractures in tectonically active regions and/or when the waveguide is not continuous, as in the case of abrupt crustal thickness variations (AKI, 1980a;

McNamara *et al*., 1996). Finally, source mechanism can determine the amplitude of *Lg*. Pure explosion sources theoretically do not generate shear energy and would not generate significant *Lg* amplitude arrivals on regional seismograms.

Motivation for our study can be observed in Figure 1. The top panel shows three separate regional seismograms, recorded at the short-period center element of the Sonseca array in central Spain (station ESDC), from three separate sources. The bottom panel shows the region of interest in our study with continental areas of Africa, Europe and the Middle East and the deep ocean basins (>1 km) of the Atlantic and Indian Oceans, and the Mediterranean, Black and Red Seas. From

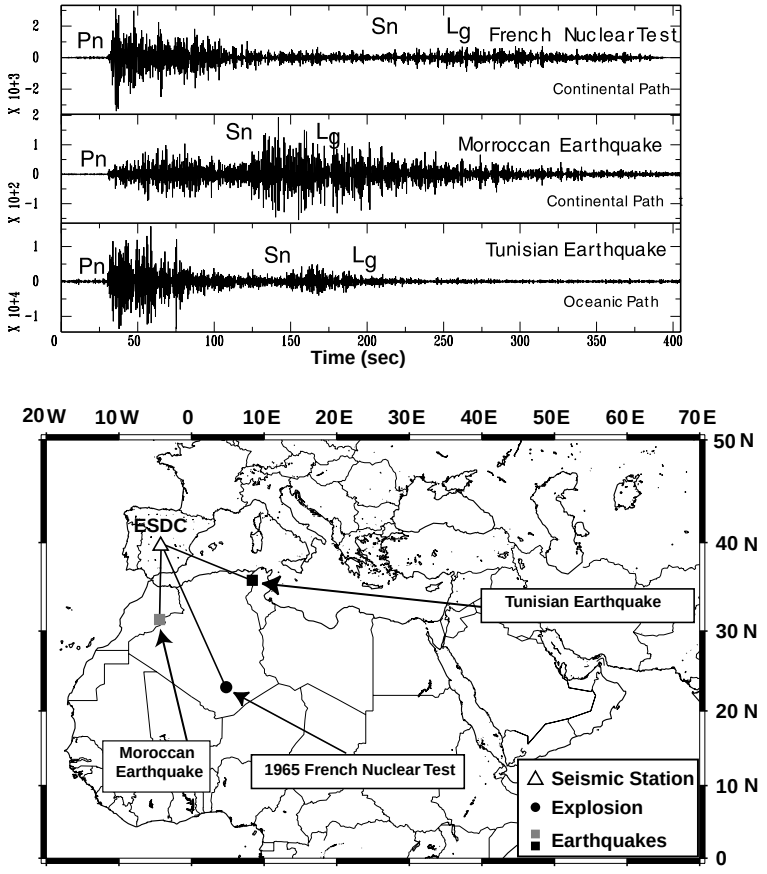

Figure 1

The top panel shows three separate regional seismograms recorded in Spain at station ESDC, from three separate sources bandpass filtered from 1–5 Hz. The sources are a 1965 French nuclear test, an earthquake from Morocco with a dominantly continental propagation path and an earthquake from Tunisia with a dominantly oceanic propagation path. The bottom panel illustrates the region of interest in our study with continental areas of Africa, Europe and the Middle East and the deep ocean basins (>1 km) of the Atlantic and Indian Oceans, and the Mediterranean, Black and Red Seas. Note the relative amplitude variations between *Pn* and *Lg* within the three seismograms.

previous, qualitative studies (KADINSKY-CADE *et al.*, 1981; RODGERS *et al.*, 1997) we anticipate significant lateral variation of *Lg* propagation throughout the region. For example, it is well established that the stable continental interior of Northern Africa has extremely high values of *Lg* coda *Q* (XIE and MITCHELL, 1990; MITCHELL, 1995). For this reason we expect the continental interiors within the region, such as Northern Africa and the Arabian Peninsula, to be imaged as having very efficient *Lg* propagation. Conversely, it is also well established that *Lg* does not propagate across deep ocean basins (ZHANG and LAY, 1995). For this reason we expect that the deep ocean basins of the Pacific and Indian Oceans will be imaged as having inefficient to absent *Lg* propagation. In addition there is considerable previous work demonstrating that the oceanic crust underlying the deep seas within the region, block *Lg* propagation. For example, SHAPIRO *et al.* (1996) have shown that the deep portions of the Mediterranean Sea do not efficiently propagate *Lg* and the Black and Caspian Seas have been shown to block *Lg* transmission (KADINSKY-CADE *et al.*, 1981; RODGERS *et al.*, 1997; MANGINO and PRIESTLEY, 1998). We have the opportunity to compare the numerous previous results to our maps.

The top panel of Figure 1 clearly demonstrates that significant variation of *Lg* amplitudes are observed within the region of interest. Note the relative amplitude variations between *Pn* and *Lg* within the three seismograms. As expected the 1965 French nuclear test, with a dominantly continental path, shows very weak to absent *Lg* energy. Such weak *Lg* amplitudes relative to *Pn* are a source characteristic of explosions and are often used to discriminate them from earthquakes (e.g., WALTER *et al.* 1995; HARTSE *et al.*, 1997). In contrast, an earthquake from eastern Morocco, with a similar path traversing the continental crust beneath the Alboran Sea, shows relatively large *Lg* amplitude relative to *Pn*. Finally, the seismogram from an earthquake in northern Tunisia manifests weak to absent *Lg* energy and closely resembles the seismogram from the French nuclear test. This is expected for earthquakes crossing structure that blocks or severely attenuates *Lg*, such as the oceanic path in this case. The Tunisian earthquake clearly demonstrates the difficulties encountered in discriminating between naturally occurring earthquakes and nuclear explosions for the CTBT, if regions that block or severely attenuate *Lg* are not well established and accounted for. With this in mind we map the lateral propagation characteristics of *Lg* in the vast region of the Tethys collision zone. This is a complex tectonic region resulting from the convergence of the African and Arabian plates with southern Eurasia. The region includes the Middle East, the Mediterranean Sea, Southern Europe and Northern Africa.

Waveform Data

We collected data from nearly 4000 moderate to large earthquakes ($m_b > 4.0$) recorded at over 100 seismic stations, sparsely distributed throughout the entire region. The distribution of earthquakes and recording stations is shown in Figures

2a, b and c. We used only crustal events with reported depths less than 40 km that occurred between 1990–1997. Event locations, origin times and magnitudes were obtained from the United States Geological Survey's (USGS) preliminary determination of epicenters (PDE) catalogs. As shown in Figure 2, seismicity across the region is not uniform. Earthquakes are concentrated in specific tectonic regions such as the subduction zones of the Mediterranean Sea and Southern Europe, the Caucasus Mountains, the Zagros thrust of western Iran, the Turkish-Iranian Plateau, to the east in the Hindu Kush and Pamirs continental collision zones, surrounding the Caspian Sea and also the active spreading centers of the Red Sea and East African Rift. Large stable continental interiors such as Northern Africa and the Arabian Peninsula have little seismicity and consequently few recording stations.

Data sources include 3-component broadband stations operated within permanent networks (WWSSN, MEDNET, GEOSCOPE, GSN), and broadband, 3-component stations from various portable deployments (Saudi Arabian PASSCAL array (VERNON *et al.*, 1996), Caspian Sea (MANGINO and PRIESTLEY, 1998)). Generally, these stations operated using Streckheisen STS2 or Guralp CMG3 and/or 40T sensors recorded at either 20 or 40 samples/sec. Such instruments are broadband and have a flat velocity response ranging from about 0.02–0.01 Hz to 10–30 Hz. Additional waveform data were obtained from vertical-component short-period stations operated in permanent and temporary arrays (Sonseca, Bilbasi). These instruments generally are operated as an array of borehole sensors and have a peak response of 1 Hz.

A large majority of waveform data was obtained through the IRIS data management center and is currently archived at Lawrence Livermore National Laboratory. The remainder of the data used in this study was obtained from individual network operators. Many stations were included that operated at different times, also the region of interest is very large. Consequently all stations do not record events shown in Figure 2.

Amplitude Measurement and Data Selection Criteria

To obtain amplitude measurements we first integrated the vertical component, raw velocity seismogram to displacement. Selection of the vertical component is based on two reasons. First, we generally observe that *Lg* energy is distributed nearly evenly across all three components of motion (MCNAMARA *et al.*, 1996). Second, all single component array stations, included in this study, recorded only vertical motion. The broadband stations operate using three-components. However, for consistency between stations, all amplitude measurements were made on the vertical component of motion. Since regional arrivals, such as *Lg*, are generally best observed at shorter periods, the broadband displacement seismograms were then filtered with a two-pole, two-pass, Butterworth filter using a passband from 0.5 to 5.0 Hz. It was

not necessary to filter the 1 Hz short-period seismograms. Each filtered and short-period seismogram was then smoothed about the mean of a 10-sample moving window. Next, we determined the seismogram envelope $E(t)$ using:

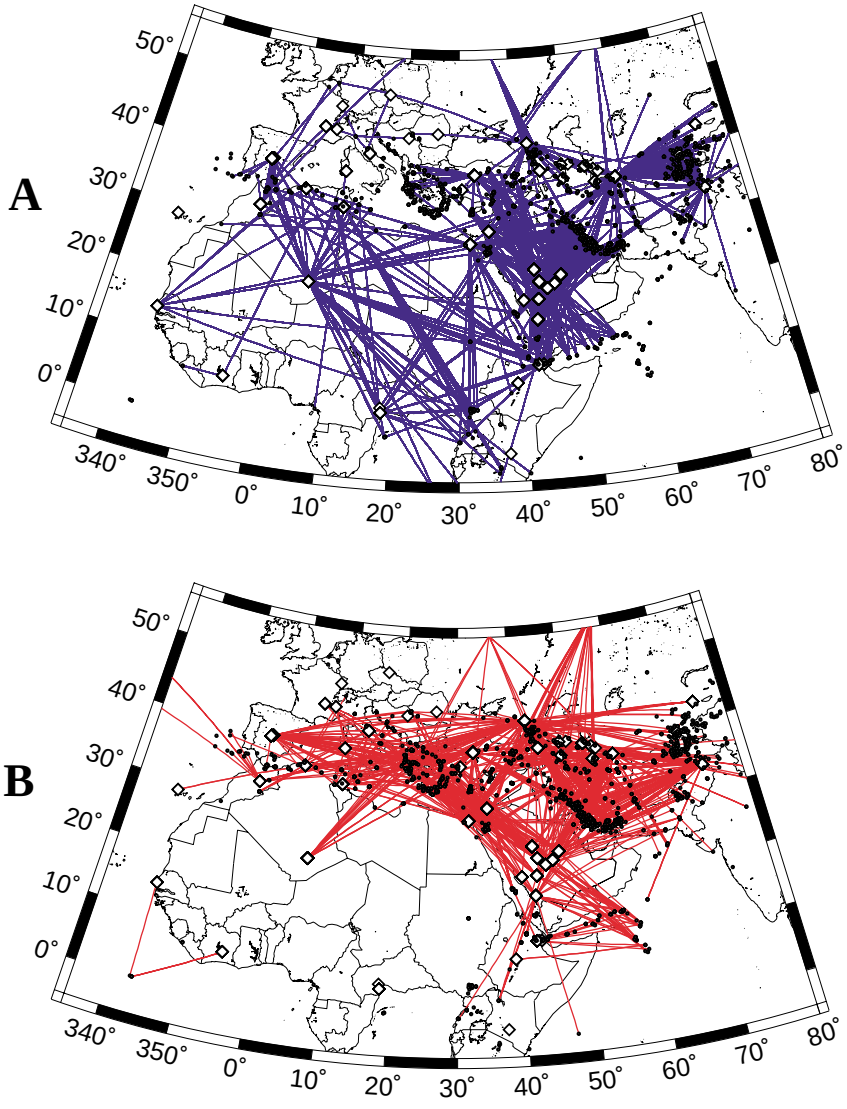

Figure 2
Maps showing the distribution of 3868 earthquakes (black circles), 108 stations (white diamonds) used in this study. Also shown are 3547 color coded raypaths reduced from 8457 after the data selection criteria were applied. (a) Raypaths with efficient *Lg* propagation. (b) Raypaths with absent *Lg* propagation. (c) Raypaths with inefficient to weak *Lg* propagation.

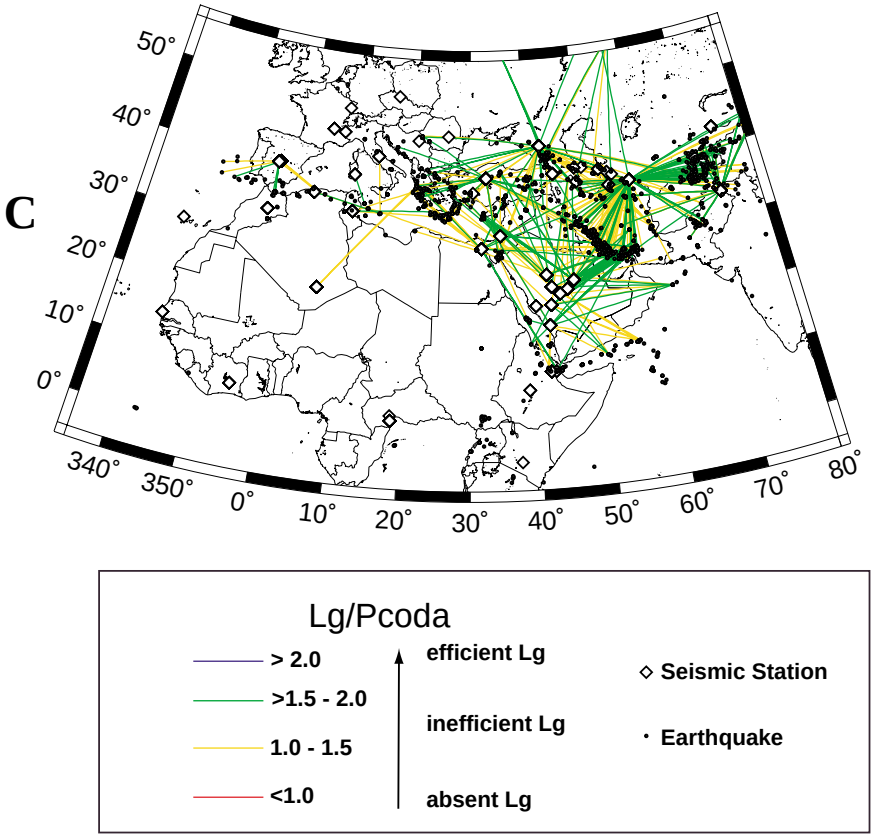

Figure 2C

$$E(t) = [A(t)^2 + H(t)^2]^{0.5} \quad (1)$$

where $A(t)$ is the smoothed, bandpassed time series and $H(t)$ is its Hilbert transform. We then measured root-mean-squares (RMS) amplitudes of the envelope function within the following group velocity windows: pre-event noise (origin time-10 km/s), *P-coda* (5.8–4.8 km/s) and *Lg* (3.6–3.0 km/s) (Fig. 3). In some cases, due to possible errors such as event location and/or depth, these windows were inappropriate and the data were not included. We also encountered numerous examples of *Sn* to *Lg* conversion for several raypaths traversing the Mediterranean Sea (SHAPIRO *et al.*, 1996). In these cases the *Lg* phase was always significantly faster than 3.6 km/s, rendering our velocity window inappropriate. Amplitude measurements, using these data, were also not included in further analysis of *Lg* propagation efficiency.

After visually inspecting all seismograms and obtaining amplitude measurements in the three-group velocity windows, amplitude ratios were computed. The *P-coda*/*pre-event noise* mean amplitude ratio was used to assess the overall signal strength of the seismogram. For inclusion in the propagation efficiency analysis we required a *P-coda*/*noise* ratio of 2 or greater. The *Lg*/*P-coda* ratio proved to be most useful for quantitatively assessing the propagation of *Lg*. We selected the *P-coda* window in order to isolate scattered energy arriving after the main regional *Pn* and *Pg* arrivals and before *Sn*. We found that normalizing *Lg* amplitude by the *P-coda* rather than *Pn* and/or *Pg* was more stable, since it is not as sensitive to source depth, focal mechanism radiation pattern and upper mantle attenuation. Using the *P-coda* amplitude, rather than the individual regional phase amplitudes (*Pn*, *Pg*) to form the ratio, allows for isolation and more accurate measure of amplitude variation of the *Lg* phase. Finally, normalizing with amplitude ratios is also required because of the inclusion of numerous instrument types with uncertain response information and to remove source-size effects.

Mapping the Lateral Variation of Lg Propagation Efficiency

Upon initial inspection of the regional seismograms, it becomes readily apparent that *Lg* amplitude can vary dramatically throughout the region of interest. For example, Figure 3 demonstrates the wide range of *Lg*/*P-coda* amplitude ratios that can be expected. For an earthquake in Morocco, recorded in southern Algeria, (92.297.09.11.09 at TAM) the *Lg* arrival is over 17 times larger than the energy contained within the *P-coda* (Fig. 3). This is likely due to the high *Q* homogeneous nature of the stable interior continental crust. In comparison, for an event of similar magnitude with a raypath of similar length, in the tectonically complex region of the Caucasus Mountains between the Caspian and Black Seas (90.215.11.57.13 at KIV), the average amplitude of the *P-coda* is three times larger than *Lg* (Fig. 3). This strongly suggests that the crustal structures associated with the Caucasus Mountains severely inhibit *Lg* transmission.

Raypath maps. As an initial step in understanding the spatial distribution of *Lg* propagation we map event/station raypaths, color coded, according to the measured *Lg*/*P-coda* amplitude ratio (Fig. 2). We are able to observe *Lg* within a wide range of path lengths, from hundreds to thousands of kilometers. We eliminated paths with epicentral distances less than 150 km because it was difficult to get adequate separation of *Lg* from other regional *S* phases. The upper path length bound was more difficult to determine because significant *Lg* energy was observed for several paths as long as 6000 km traversing Northern Africa. We defined four categories of *Lg* propagation efficiency based on the *Lg*/*P-coda* amplitude ratio. *Lg* is considered efficient when the *Lg*/*P-coda* ratio is greater than 2.0 and is mapped with blue lines in Figure 2a. *Lg* is considered absent when the *Lg*/*P-coda* ratio is less than 1.0 and

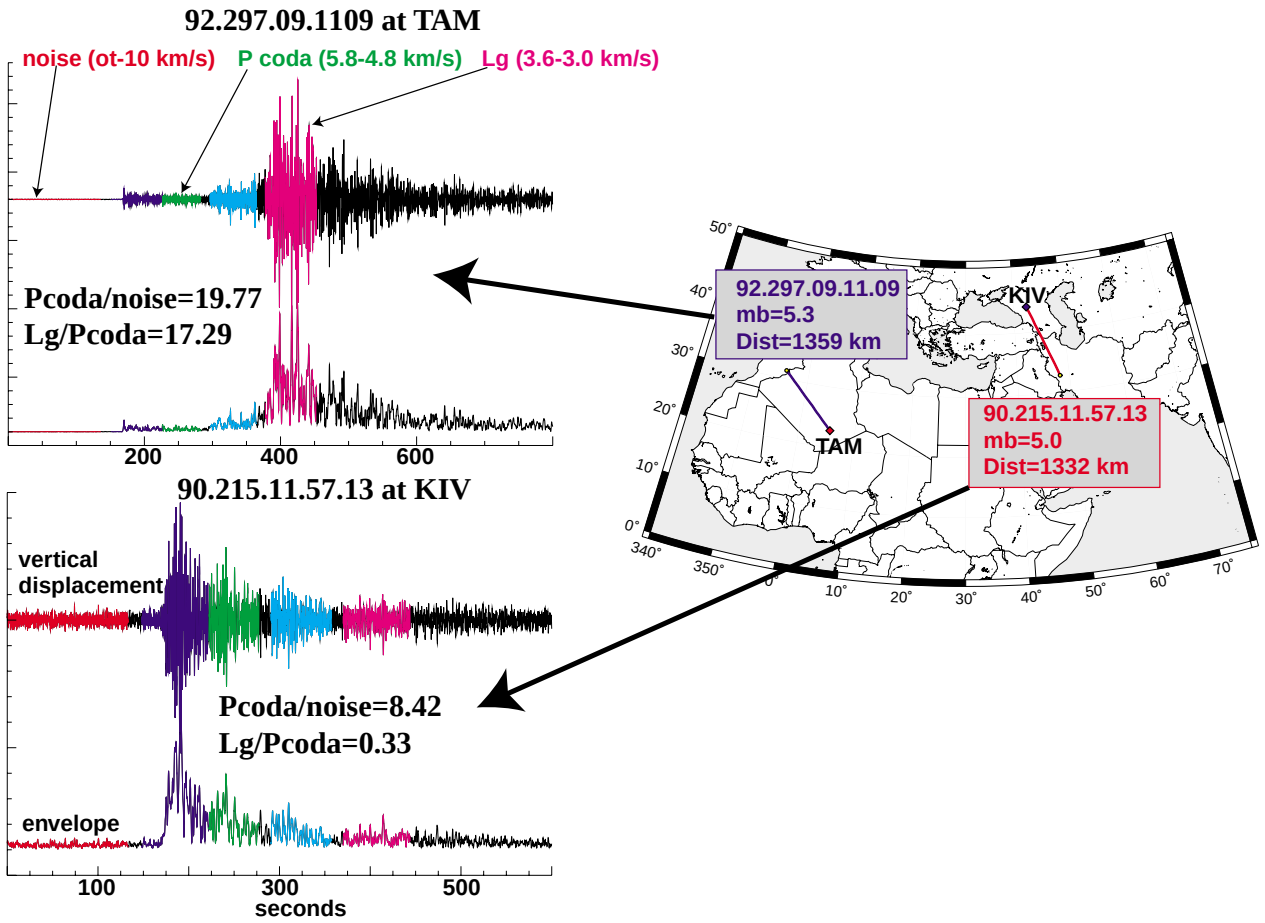
92.297.09.1109 at TAM
noise (ot-10 km/s)
P coda (5.8-4.8 km/s)
Lg (3.6-3.0 km/s)
Pcoda/noise=19.77
Lg/Pcoda=17.29
200
400
600
90.215.11.57.13 at KIV
vertical displacement
Pcoda/noise=8.42
Lg/Pcoda=0.33
envelope
100
300
500
seconds
92.297.09.11.09
mb=5.3
Dist=1359 km
KIV
TAM
90.215.11.57.13
mb=5.0
Dist=1332 km
50°
40°
30°
20°
10°
0°
340°
350°
10°
20°
30°
40°
50°
60°
70°

is mapped with red lines in Figure 2b. Weak and inefficient *Lg* propagation ($Lg/P\text{-}coda = 1.0 < 2.0$) is mapped in Figure 2c.

The raypath maps show significant variation of *Lg* propagation efficiency throughout the region. We observe strong *Lg* in the stable continental interiors of Northern Africa and the Arabian Peninsula, and clearly absent *Lg* for most paths traversing the Mediterranean Sea. By visual inspection of the raypath maps it is difficult however, to completely identify the regions where *Lg* is absent and even more difficult to interpret the regions of weak and inefficient propagation. For this reason we now present our method to more clearly image the lateral variation of *Lg* propagation efficiency.

Maximum Lg/P-coda cell maps. To better constrain the spatial distribution of *Lg* propagation characteristics we attempt to visually simplify this information by imaging crustal structures that efficiently propagates *Lg* and significantly diminishes the amplitude of *Lg*. The imaging of such amplitude anomalies is achieved by defining a grid of cells that covers the entire region of interest. We trace *Lg* rays for each event/station pair, which is simply the great circle path, and attribute to each cell a value equal to the maximum value of the *Lg/P-coda* amplitude ratio for all paths traversing that particular cell. If all rays traversing a particular cell do not contain significant *Lg* energy ($Lg/P\text{-}coda < 1.0$), the cell is colored red (Fig. 4). Cells where only absent or inefficient *Lg* paths are present are colored from orange to yellow depending on the maximum value (Fig. 4). Cells that allow efficient to strong *Lg* propagation are colored from green to dark blue (Fig. 4). By mapping the maximum *Lg/P-coda* ratio, traversing the cell, we are able to negate the bias from inefficient or absent *Lg* that later propagate into regions of efficient *Lg* propagation. This method allows us to more accurately resolve the boundaries of regions of different propagation characteristics by reducing smearing, and reduces inefficient *Lg* propagation artifacts.

Figure 4 shows a map using a regularly defined grid, with 111.14 km cells, covering the entire region of interest. Raypath lengths range from 150–6000 km, unless the *Lg/P-coda* ratio is less than 1.0. In this case, the maximum allowable raypath length was reduced to 2000 km. The elimination of long paths with absent *Lg* was done to minimize normal attenuation effects and the effects of off-azimuth

◀

Figure 3

We show the bandpassed filtered (0.5–5.0 Hz), high signal-to-noise seismograms and envelope functions for two earthquakes with dramatically different *Lg* propagation characteristics. We also present examples of the velocity windows used for amplitude measurement: pre-event noise (0–10 km/s), *P-coda* (5.8–4.8) km/s and *Lg* (3.6–3.8 km/s). Event 92.297.09.11.09 ($mb = 5.3$) occurred in Morocco and was recorded in Southern Algeria (GEOSCOPE station TAM) at a distance of 1359 km. The seismogram and envelope functions show the characteristic efficient *Lg* propagation that occurs in the continental crust of Northern Africa ($Lg/P\text{-}coda = 17.29$). Event 90.215.11.57.13 ($mb = 5.0$) occurred in western Iran and was recorded at GSN station KIV at a distance of 1332 km. The seismogram and envelope functions indicate that along this path through the Caucasus Mountains *Lg* propagation is absent ($Lg/P\text{-}coda = 0.33$).

propagation. It also reduced inefficient *Lg* artifacts in regions of efficient propagation. After applying the data selection criteria discussed in the previous sections, 8257 paths were reduced to 3547 high-quality *Lg*/*P-coda* amplitude measurements. These high-quality measurements were then used to construct the map shown in Figure 4.

Mapping event/station paths, color coded to represent the *Lg* amplitude observations, is the typical technique used to display this type of information. However, in our case, with several thousand observations, we find mapping the maximum *Lg*/*P-coda* by cell provides a clearer and more easily interpretable view of the regional variation of *Lg* propagation. In effect, we are mapping the large-scale, first-order *Lg* blockage and propagation efficiency features. The most significant observation from our data set is that *Lg* propagation efficiency varies considerably and regions that do not effectively transmit *Lg* energy can be roughly correlated to tectonic structures. Features shown in Figure 4 are consistent with previous studies and clearly identify regions of inefficient to absent *Lg*, such as the Mediterranean Sea as well as regions of efficient to strong *Lg* propagation, such as Northern Africa and the Arabian Peninsula (ROGERS *et al.*, 1997).

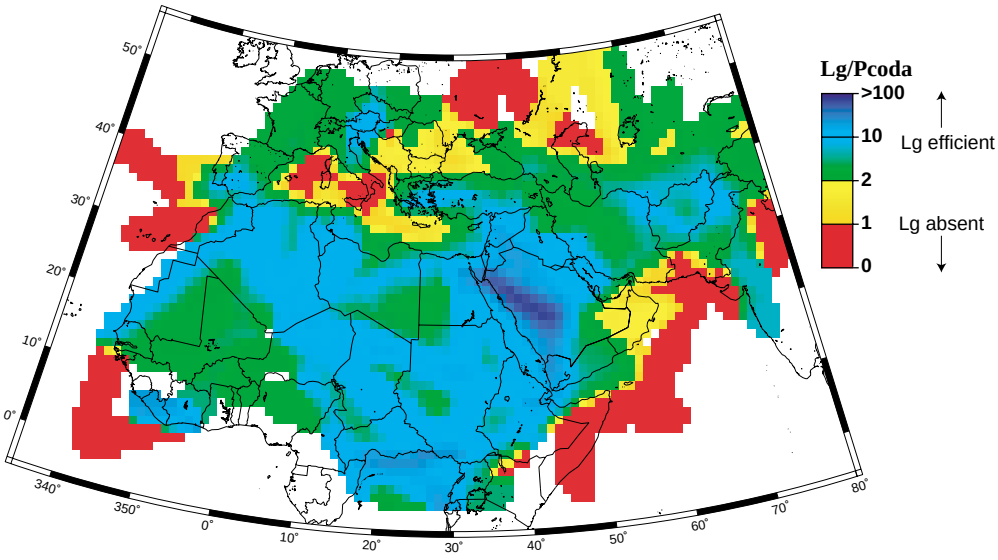

Figure 4
A map showing the results of our empirical *Lg* propagation efficiency mapping technique. Cells are color coded by the maximum *Lg*/*P-coda* value that traverses a particular cell. In this example the entire region is divided into 111.14 km cells and 3547 raypaths are used to construct the map. The maximum path length was 6000 km unless *Lg* was absent from the trace (Lg/P-coda $<$ 1.0). In this case the maximum allowable path length was reduced to 2000 km. Only large-scale features are imaged in this map. For example, the Mediterranean Sea propagates *Lg* inefficiently while continental interiors such as Northern Africa and the Arabian Peninsula show very efficient *Lg* propagation.

Resolution. A first-order measure of data set resolution can be obtained by inspecting the raypath distribution within the region (Figs. 2a, b, c). Regions with both high raypath density and good azimuthal distribution will have the best resolution. Figure 5 is a map showing the number of raypaths traversing each cell. Raypath density is greatest in the Middle East, including Iran, Iraq, the Caucasus and southern Caspian region. The Arabian Peninsula has relatively good raypath density while Northern Africa, the Mediterranean and Europe are the poorest resolved regions. In these areas, where raypath density and azimuthal distribution is limited, as in Northern Africa, streaking occurs and the colored cells will resemble the event/station ray path map (Fig. 4). Only larger scale features, on the order of hundreds of kilometers (i.e., Mediterranean Sea), are resolvable. We will show, in later sections, that by applying further data selection criteria, to reduce multipathing, we can significantly increase the resolution of our data set. In areas of good raypath coverage we are able to image *Lg* propagation features on the order of 100 km and less (i.e., Caspian Sea and Red Sea).

Previous Lg propagation efficiency mapping methods. Numerous researchers have attempted to use the propagation characteristics of *Lg* to map crustal heterogeneity in a variety of regions throughout the world. For many years now, these studies have relied on qualitatively accessing the amplitude of *Lg* and then analyzing individual propagation paths in search of blockage features. For example RUZAIKIN *et al.* (1977) observed that the Tibetan Plateau does not effectively propagate *Lg* energy by

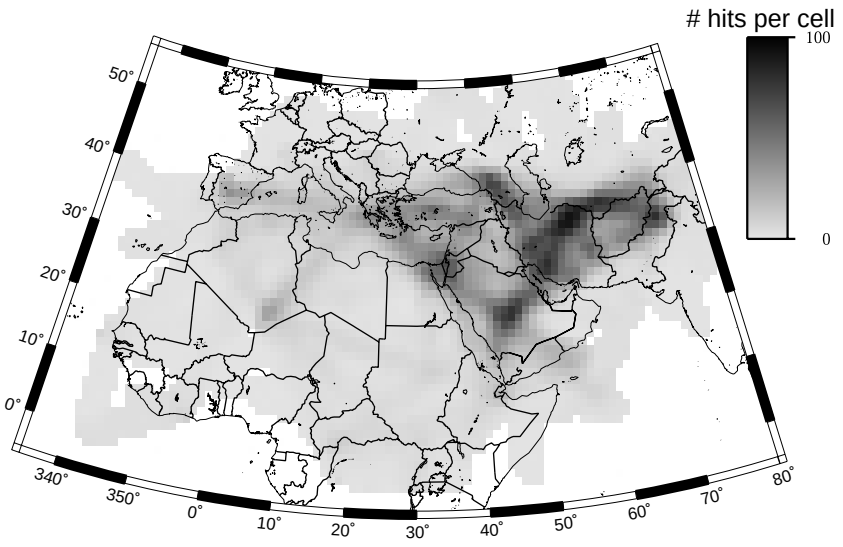

Figure 5
A map indicating the number of raypaths per cell. This points to the data set's ability to resolve *Lg* propagation features. The best coverage is in the seismically active Middle East and in the Arabian Peninsula. All shaded cells have at least 3 raypath hits.

simple visual inspection of *Lg* amplitudes. Later studies added more data (NI and BARAZANGI, 1983) and a slightly more quantitative approach, by measuring amplitude ratios (MCNAMARA *et al.*, 1996), to further refine the *Lg* propagation features in the Tibetan Plateau. A similar history exists in the Middle East. Early raypath mapping results of KADINSKY-CADE *et al.* (1981) were updated and improved by the more quantitative work of RODGERS *et al.* (1997). Qualitative raypath mapping has been an effective method for understanding first-order *Lg* propagation features.

Attempts to quantitatively assess the propagation quality of *Lg*, and then map it in a detailed grid, are relatively uncommon. One early example is KENNETT *et al.* (1985) who mapped crustal heterogeneity in the North Sea basin with a back-projection inversion scheme. *Lg* amplitude was assessed and assigned a code from 1–5 based on its amplitude relative to *Sn*. Their scheme included intermediate *Lg* amplitudes, as was an extension of the classification system defined earlier by GREGERSEN (1984). Heterogeneity values were then assigned to cells within the gridded region, based on the *Lg* classification codes of all paths traversing each cell. While KENNETT *et al.* (1985) represents an improvement over qualitative approaches, we found it limited in two ways. First, the *Lg* amplitude classification system is significantly less quantitative than a simple measure of normalized amplitude. Second, *Sn* amplitude is sensitive to source depth, radiation pattern and upper mantle *Qs*. Consequently, an assessment of crustal heterogeneity is significantly biased by the inclusion of *Sn* since the variations of *Lg* amplitude and crustal *Q* are not easily isolated.

Using a method more similar to ours, CAMPILLO *et al.* (1993) mapped the variation of *Lg* amplitudes in the southwestern region of the Alpine Range. They divided the region into a grid and attributed to each cell the mean value of the *Lg*/*Pn* amplitude ratios computed for all paths traversing the cell, weighted by their length in the particular cell. This approach represents an improvement, but is limited for two reasons. First, unlike the scattered energy of the *P-coda*, *Pn* amplitude is very sensitive to source depth, radiation pattern and upper mantle *Qp*, and velocity gradient. Consequently, the inclusion of *Pn* rather than the P-coda significantly biases an assessment of crustal heterogeneity, and variations of *Lg* amplitude are not easily isolated. Second, the mean amplitude ratio, rather than the maximum, will bias amplitude values in regions of efficient *Lg* propagation unrealistically low. This occurs when a path with weak to absent *Lg* energy traverses into a region of high *Q* or efficient *Lg* propagation. By using the maximum amplitude ratio we are essentially removing the effect an absent *Lg* (small *Lg*/*P-coda*) propagation path in regions of strong *Lg* (large *Lg*/*P-coda*) propagation energy. This is not the case when these weak or absent *Lg* amplitudes are included to compute the mean amplitude ratio assigned to a particular cell. Therefore, mapping the maximum *Lg*/*P-coda* value traversing a given cell is a quantitative and more accurate representation of the crustal heterogeneity responsible for the observed *Lg* amplitudes.

Technique limitations. It is important to note that our technique has several limitations. For example, we assume that any attenuating or blocking structure is isotropic. Specifically, the azimuth of propagation does not effect Lg propagation efficiency. While this is a simple assumption pertaining to the structure of the crust, it appears to be adequate enough to determine the first-order propagation characteristics of the region. Extracting more subtle features such as anisotropic behavior simply requires analysis of individual raypaths, in addition to the maximum *Lg*/*P-coda* cell maps.

Second, the selection of our *P-coda* velocity window (5.8–4.8 km/s) may allow some contamination from slowly propagating direct *Pg* arrivals. Our goal was to normalize *Lg* amplitudes with the signal closest to the phase (*Lg*) using a narrow window uncontaminated by other direct phases (*Pn*, *Pg*, *Sn*) yet long enough to provide a good RMS amplitude. While the window bound of 5.8 km/s may allow some leakage of *Pg* energy, the bulk of the window contains scattered *P-coda*.

Our approach also does not account for the effects of ray-bending and multipathing. Because the raypath of a regional phase, such as *Lg*, will bend around low velocity structures, the lateral extent of regions that attenuate *Lg* transmission may be underestimated. The longer the raypath the more serious the effect of ray-bending. This effect can be observed in both the Red Sea and Caspian Sea. Both are known to severely attenuate the transmission of *Lg*. However they do not appear as blocking regions when long raypaths are included in the low-resolution cell map (Fig. 4). To eliminate the effects of ray-bending and the consequent reduction of anomaly area in the next section, we will show, individual sub-regions with a finer grid and shorter, regional, raypaths.

Finally, our approach requires very high quality data and is heavily dependent on accurate amplitude ratio measurements. Since we use only the single maximum amplitude ratio to define the value of a particular cell, rather than an average of all paths traversing the cell, a single poor-quality amplitude measurement can seriously degrade the reliability of the image within that region. By applying our strict data selection criteria we have removed a considerable amount of erroneous paths, resulting in a data set of high quality *Lg*/*P-coda* amplitude ratios.

Regional Observations Lg Propagation Efficiency

We will now discuss the efficiency of *Lg* propagation within four sub-regions, the Western Mediterranean and Alboran Seas (Fig. 6), the Red Sea and Arabian Peninsula (Fig. 7), the Caspian Sea (Fig. 8) and the Eastern Mediterranean and Black Seas (Fig. 9). In this section we will compare our results with those of previous qualitative studies and demonstrate that our technique successfully images heterogeneous crustal structure responsible for the observed *Lg* amplitude variations. We will also demonstrate how we can enhance image features and improve resolution by

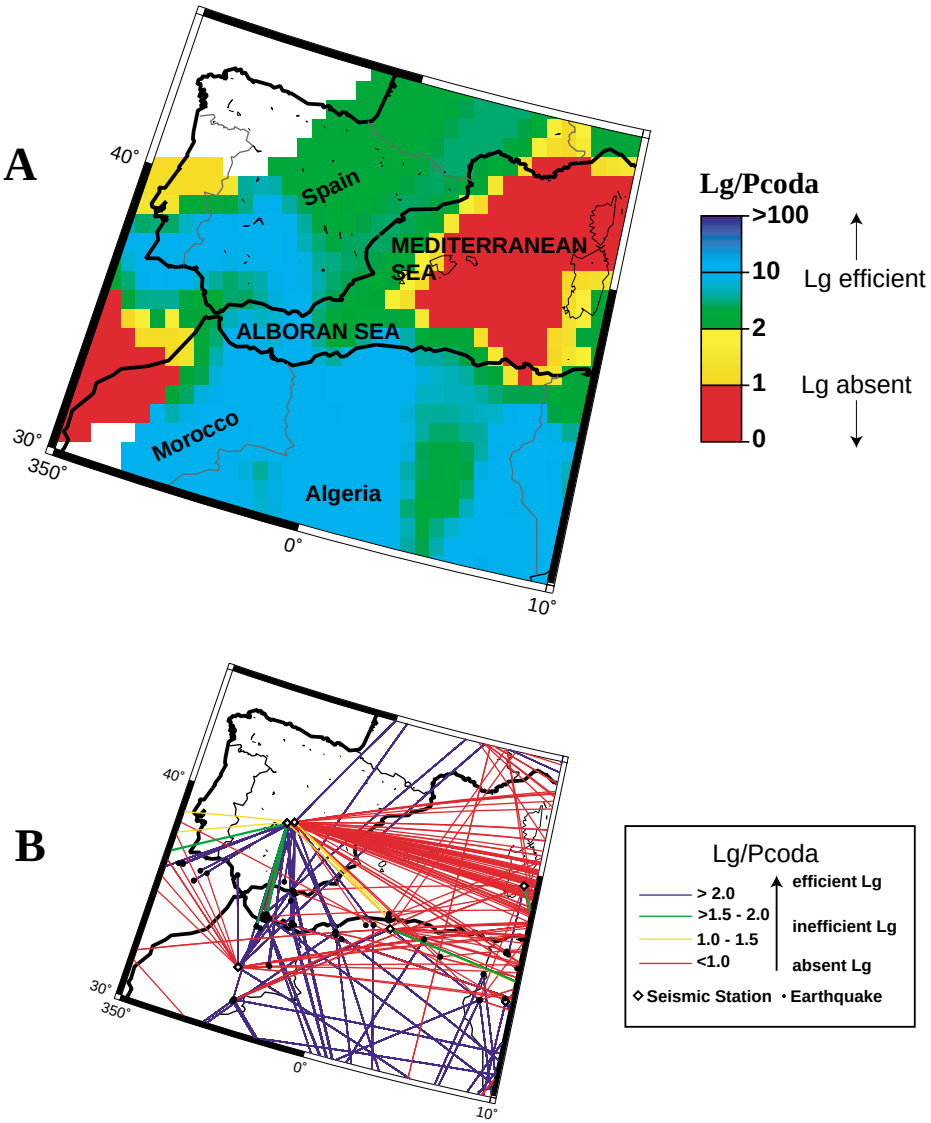

Figure 6

(a) Regional *Lg* propagation map showing the region surrounding the western Mediterranean and Alboran Seas. A finer grid (55.7 km cells) and shorter, regional raypaths lengths are used to improve resolution and allow the imaging of small-scale *Lg* propagation features. Small-scale features, such as efficient *Lg* propagation across the Alboran Sea and the sharp boundary between the Mediterranean Sea and continental Africa and Europe, are well imaged. (b) 135 regional raypaths used to construct the map in Figure 6a (maximum path length = 1500 km, maximum with absent *Lg* = 1000 km. The area containing the raypaths ranges in latitude from −20.0° to 20.0° and longitude from −20.0° to 20.0° and is slightly larger than the mapped area.

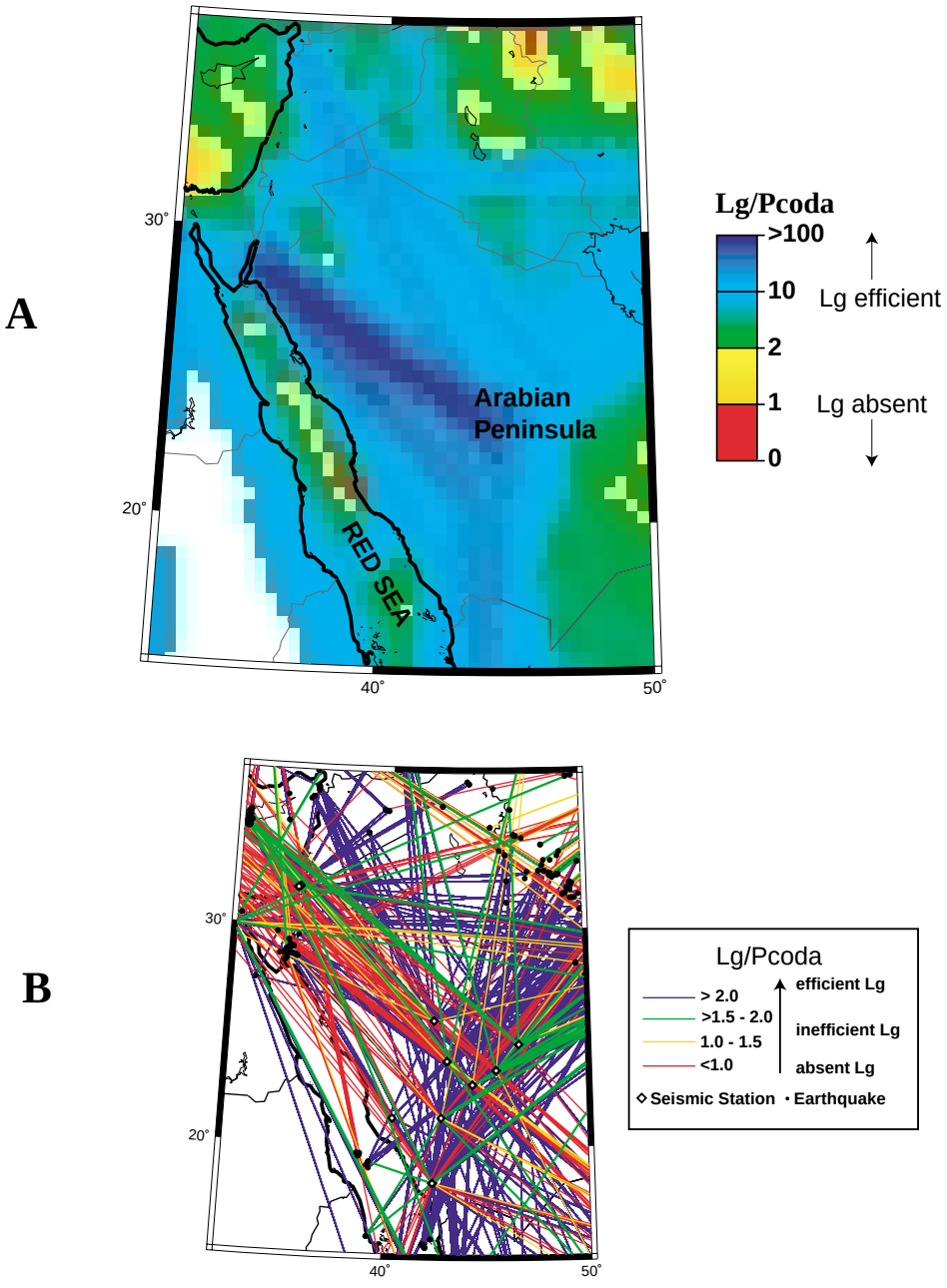

Figure 7

(a) Regional *Lg* propagation map delineating a narrow zone of absent to inefficient *Lg* propagation down the center of the Red Sea and the very efficient propagation region of the Arabian Peninsula. A finer grid (55.7 km cells) and shorter, regional raypaths lengths are used to improve the imaging of small-scale *Lg* propagation features. (b) 1247 regional raypaths used to construct the map in figure 6a (maximum path length = 2000 km, maximum with absent *Lg* = 1500 km). The area containing the raypaths ranges in latitude from 0.0° to 40.0° and longitude from 20.0° to 60.0° and is slightly larger than the mapped area.

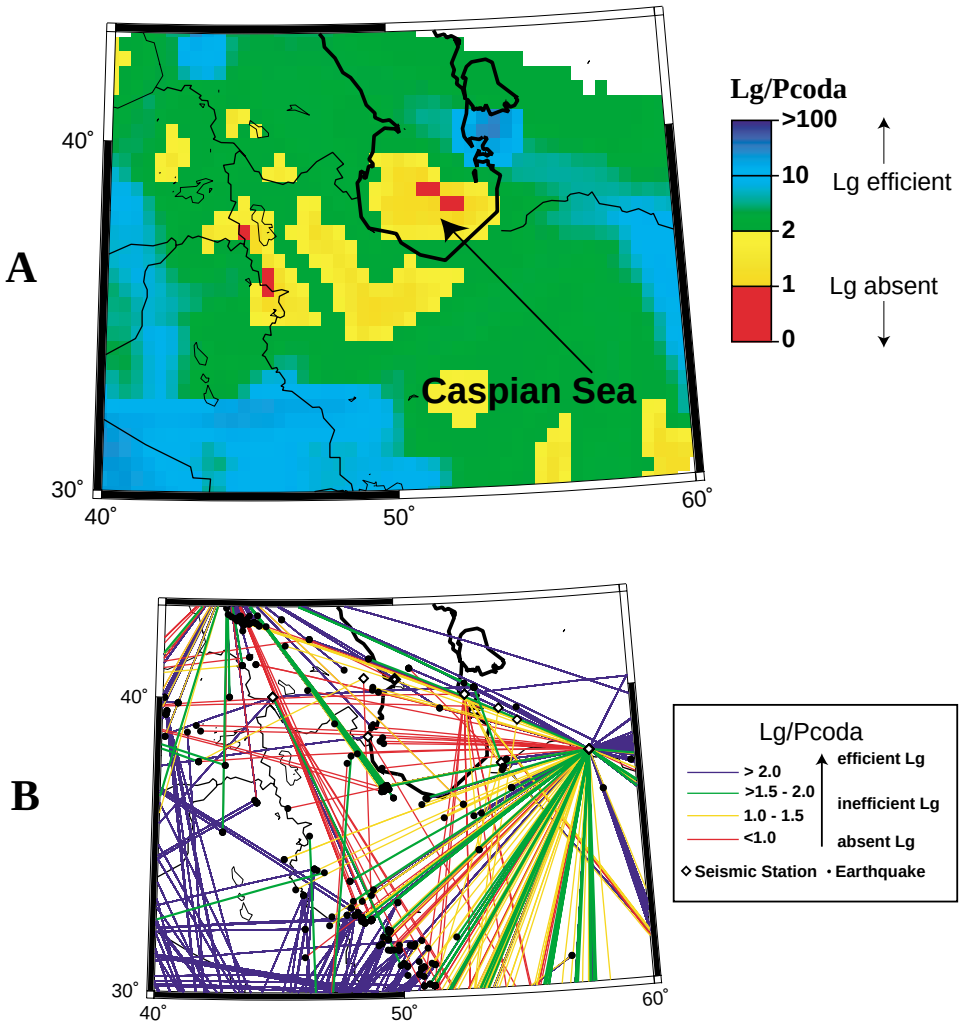

Figure 8
Regional *Lg* propagation map designating a zone of absent to inefficient *Lg* propagation in the southern Caspian Sea and Caucasus Mountains. A finer grid (55.7 km cells) and shorter, regional raypaths are used to improve the imaging of small-scale *Lg* propagation features. (b) 1009 regional raypaths used to construct the map in Figure 6a (maximum path length = 1500 km, maximum with absent *Lg* = 1000 km). The area containing the raypaths ranges in latitude from 20.0° to 50.0° and longitude from 30.0° to 70.0° and is slightly larger than the mapped area.

limiting *Lg* raypath lengths to regional distances and using a finer grid (55.7 km cells). Raypath lengths, with efficient to strong *Lg*, are limited to 1500–2000 km, depending on coverage within the particular region. Raypaths with inefficient to absent *Lg* are limited to 1000–1500 km.

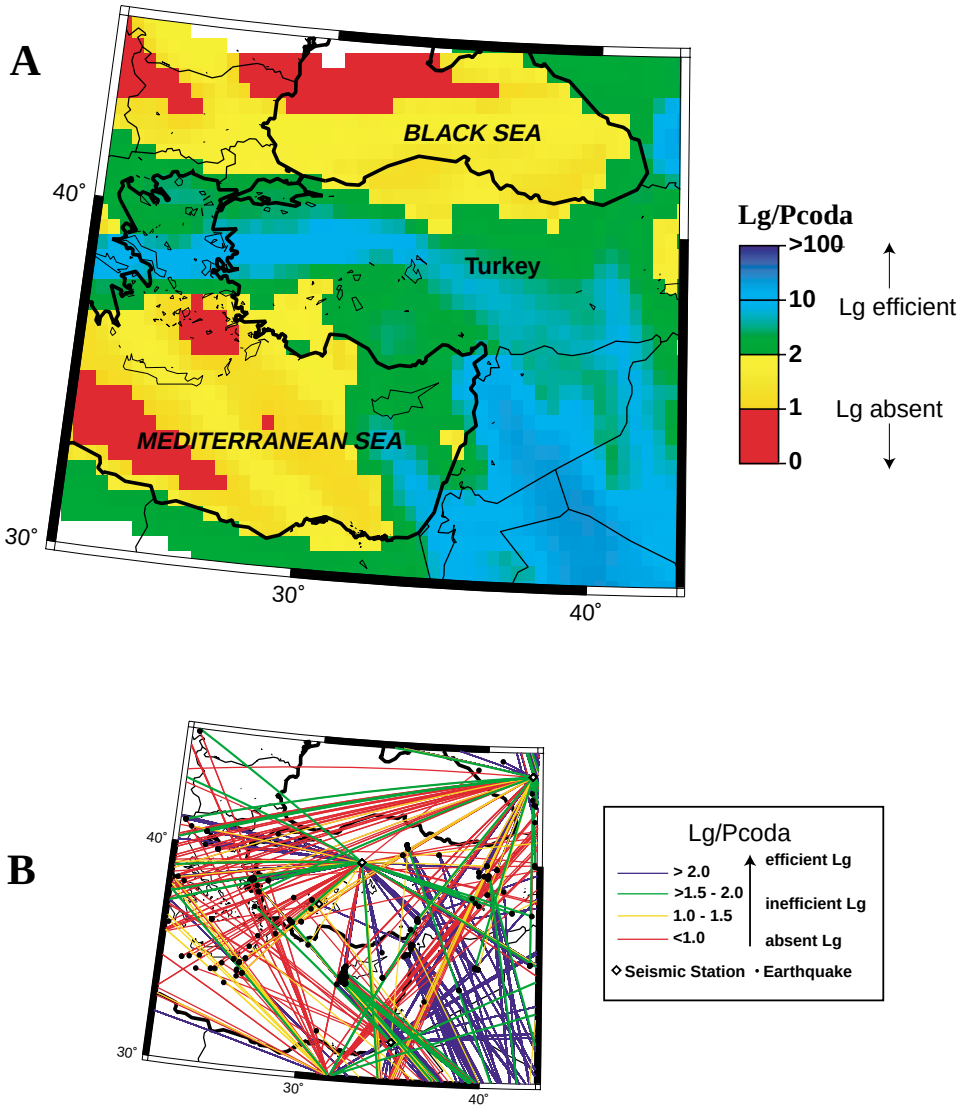

Figure 9

Regional *Lg* propagation map showing regions of absent to inefficient *Lg* propagation in the deep basins of the Mediterranean and Black Seas. *Lg* propagation is relatively efficient in Turkey, Syria, Israel, and the northern Arabian Peninsula. Also *Lg* propagation is relatively efficient in the shallow basins of the far eastern Mediterranean Sea, implying that they are underlain by continental crust. A finer grid (55.7 km cells) and shorter, regional raypaths are used to improve the imaging of small-scale *Lg* propagation features. (b) 664 regional raypaths used to construct the map in Figure 6a (maximum path length = 1500 km, maximum with absent *Lg* = 1000 km). The area containing the raypaths ranges in latitude from 20.0° to 55.0° and longitude from 15.0° to 50.0° and is slightly larger than the mapped area.

Western Mediterranean and Alboran Sea. To improve the resolution of *Lg* propagation characteristics in this region we selected 135 high-quality measurements with regional propagation distances (maximum path length = 1500 km, maximum with absent *Lg* = 1000 km) in a box ranging in latitude from −20.0° to 20.0° and longitude from −20.0° to 20.0°. These paths were used to construct the map in Figure 6. Despite the very low number of raypaths, this region clearly demonstrates how well our technique can define the boundaries between regions of different *Lg* propagation characteristics (Fig. 6). For example, it is well known that the stable continental interior of Northern Africa has extremely high values of *Lg*-coda *Q* (XIE and MITCHELL, 1990). To illustrate, we have observed strong *Lg* for individual paths as long as 5000–6000 km in this region. Such observations indicate that *Lg* propagation is very strong in Northern Africa. Conversely, the deep ocean basins of the Mediterranean do not efficiently propagate *Lg* (SHAPIRO *et al*., 1996). The deep portions of the Mediterranean are underlain by oceanic crust. It is well known that *Lg* does not propagate across deep oceanic basins (ZHANG and LAY, 1995). Figure 6 demonstrates that the efficient propagation region of Northern Africa and the inefficient propagation region of the Mediterranean Sea are clearly delineated with our mapping technique. We also observe that *Lg* propagates efficiently across the shallow Alboran Sea. This is likely due to the fact that the Alboran Sea is underlain by continental rather than oceanic crust (SEBER *et al*., 1996).

The pattern of crustal heterogeneity is less easily interpreted off the Atlantic Coast of Morocco. The blocking region is expected due to the transition from oceanic to continental crust, however, the region of efficient *Lg* propagation off the coast of Spain is not expected. This could likely be due to *Sn* to *Lg* conversions (SEBER *et al*., 1994).

The Red Sea and Arabian Peninsula. To improve the resolution of *Lg* propagation features in this region we selected 1247 high-quality regional paths (maximum path length = 2000 km, maximum with absent *Lg* = 1500 km) in a box ranging in latitude from 0.0° to 40.0° and longitude from 20.0° to 60.0°. These paths were used to construct the map in Figure 7. The largest *Lg* amplitudes observed in our crustal heterogeneity mapping were observed for paths traversing the western Arabian Peninsula. As shown in Figure 7, *Lg*/*P-coda* ratios can be a high as 100. This observation is consistent with several previous qualitative studies of *Lg* amplitude variation (KADINSKY-CADE *et al*., 1981; RODGERS *et al*., 1997) and surface wave attenuation (SEBER and MITCHELL, 1992) in the Arabian Peninsula. Using a more quantitative approach, MELLORS *et al*. (1999) analyzed regional seismogram stacks for the amplitude variation of *Lg* as a function of source location and backazimuth using data recorded at portable broadband seismic stations deployed within the Arabian Peninsula (Vernon *et al*., 1996). They noted that the largest *Lg* amplitudes were observed from events to the north in the Gulf of Aquaba and that seismograms from events located in Africa showed weak to absent *Lg* energy. This is consistent with the results of our study. The most striking feature in this map is a narrow

50–100-km wide band of inefficient *Lg* propagation. This band corresponds to the deepest portions of the northern Red Sea and indicates that raypaths traversing the Red Sea should show inefficient *Lg* propagation. We suspect that the narrow band of inefficient *Lg* propagation extends the length of the Red Sea, however, due to the limited number of earthquakes in the region and limited raypath coverage, we are unable to completely image this feature.

Caspian Sea. Previous studies that qualitatively assess *Lg* amplitude clearly show that paths traversing the southern Caspian Sea do not have significant *Lg* energy (MANGINO and PRIESTLEY, 1998; KADINSKY-CADE *et al*., 1981; RODGERS *et al*., 1997). When we limit raypaths lengths to include only regional distances (1009 paths, maximum path length = 1500 km, maximum with absent *Lg* = 1000 km) in a box ranging in latitude from 20.0° to 50.0° and longitude from 30.0° to 70.0°, the southern Caspian is clearly imaged as a region of weak to absent *Lg* propagation (Fig. 8). We also observe that the lesser Caucasus, adjacent to the Caspian Sea, are also imaged as a region of inefficient *Lg* propagation. This observation is evident in the seismogram in Figure 3 and is consistent with the previous qualitative studies discussed above. The region of *Lg* blockage in the Southern Caspian is likely larger than imaged due to *Lg* paths bending around regions of low velocity. We suspect that ray-bending will reduce the areal extent of the imaged blocking region. Due to limited shorter raypath coverage, we are not able to further improve the image resolution in this region without additional data. However, with our current data set and mapping method we are able to resolve *Lg* blocking structures in this region on the order of several hundred kilometers (Fig. 8).

Eastern Mediterranean and Black Seas. Finally, to improve the resolution of *Lg* propagation features in this region, we selected 664 high quality regional paths (maximum path length = 1500 km, maximum with absent *Lg* = 1000 km) in a box ranging in latitude from 20.0° to 55.0° and longitude from 15.0° to 50.0°. These paths were used to construct the map in Figure 9. Figure 9 clearly shows regions of absent to inefficient *Lg* propagation in the deep basins of the Mediterranean and Black Seas. In contrast, *Lg* propagation is relatively efficient in Turkey, Syria, Israel, and the northern Arabian Peninsula. These observations are expected and consistent with previous qualitative *Lg* amplitude studies (KADINSKY-CADE *et al*., 1981; RODGERS *et al*., 1997). In addition, *Lg* propagation is relatively efficient in the shallow basins of the eastern Mediterranean Sea, implying that they are underlain by continental crust.

Conclusions

The patterns of crustal heterogeneity that we have imaged, using *Lg* amplitude variations, correlate well with the major tectonic features of the region and are consistent with several previous investigations. From this we conclude that our

empirical and qualitative method of mapping maximum *Lg*/*P-coda* values can successfully image relatively small-scale, detailed crustal structure. We have shown in our regional analysis that our approach can resolve *Lg* blocking features on the order of 50–100 km in regions of good raypath distribution and coverage (e.g., South Caspian Sea and Red Sea).

The inefficient propagation and blockage of *Lg* from earthquake sources, by complex tectonic features in the Middle East and Northern Africa, pose serious challenges for the utility of the *Lg* phase in CTBT monitoring. An accurate understanding of the factors that affect the variation of *Lg* amplitude and propagation characteristics is important to enable effective discrimination between earthquakes and nuclear explosions. With our mapping method, accurate determination of the expected *Lg* amplitude variations, due to crustal structure within a particular region, can be quickly obtained and applied to discrimination efforts. Also, results from our imaging can be used to screen out regional paths that traverse *Lg* blocking regions. This may be required to accurately obtain crustal *Q* parameters using the *Lg* phase. For example, the inclusion of paths where *Lg* is absent from the seismogram would significantly bias tomographic *Q* models.

The resultant set of *Lg* propagation maps from our empirical approach has been demonstrated to be easily interpreted in terms of crustal structure, and can successfully image detailed blockage features often missed by analysis of raypaths alone. Furthermore it is extremely useful for monitoring the Comprehensive Test-Ban Treaty.

Acknowledgments

The authors would like to thank J. Lahr, P. Earle and 2 anonymous reviewers for comments that improved our manuscript.

Thanks to Terri Hauk and Stan Ruppert for data acquisition and archiving. Work performed under the auspices of the U.S. Department of Energy by the Lawrence Livermore National Laboratory under contract number W-7405-ENG-48. This work was supported by DOE LLNL grant #GI 99-82 to the University of Alaska. Maps were created using GMT (WESSEL and SMITH, 1990).

REFERENCES

AKI, K. (1980a), *Scattering and Attenuation of Shear Waves in the Lithosphere*, J. Geophys. Res. *85*, 6496–6504.

AKI, K. (1980b), *Scattering and Attenuation of Shear Waves in the Lithosphere from 0.05 to 25 Hz*, Phys. Earth Planet. Interiors *21*, 50–60.

BOUCHON, M. (1982), *The Complete Synthesis of Seismic Crustal Phases at Regional Distances*, J. Geophys. Res. *87*, 1735–1741.

EWING, W., JARDETZKY, W., and PRESS, F. (1957), *Elastic Waves in Layered Media* (McGraw-Hill, New York, 380 pp).

CAMPILLO, M., FEIGNIER, B., BOUCHON, M., and BETHOUX, N. (1993), *Attenuation of Crustal Waves Across the Alpine Range*, J. Geophys. Res. *98*, 1987–1996.

GUTENBERG, B. (1955), *Channel Waves in the Earth's Crust*, Geophysics *20*, 283–294.

GREGERSEN, S. (1984), *Lg Wave Propagation and Crustal Structure Differences near Denmark and the North Sea*, Geophys. J. R. Astron. Soc. *79*, 217–234.

HARTSE, H., TAYLOR, S. R., PHILLIPS, W. S., and RANDALL, G. E. (1997), *A Preliminary Study of Regional Seismic Discrimination in Central Asia with an Emphasis on Western China*, Bull. Seism. Soc. Am. *87*, 551–568.

HERRIN, E., and RICHMOND, J. (1960), *On the Propagation of the Lg Phase*, Bull. Seism. Soc. Am. *50*, 197–210.

KADINSKY-CADE, K., BARAZANGI, M., OLIVER, J., and ISAAKS, B. (1981), *Lateral Variations of High-frequency Seismic Wave Propagation at Regional Distances across the Turkish and Iranian Plateaus*, J. Geophys. Res. *86*, 9377–9396.

KENNETT, B. (1986), *Lg Waves and Structural Boundaries*, Bull. Seismol. Soc. Am. *76*, 1133–1141.

KENNETT, B., GREGERSEN, S., MYKKELTVEIT, S., and NEWMARK, R. (1985), *Mapping of Crustal Heterogeneity in the North Sea Basin via the Propagation of Lg-Waves*, Geophys. J. R. Astr. Soc. *83*, 299–306.

KNOPOFF, L., SCHWAB, F., and KAUSSEL, E. (1973), *Interpretation of Lg*, Geophys. J. R. Astron. Soc. *33*, 389–404.

MANGINO, S., and PRIESTLEY, K. (1998), *The Crustal Structure of the Southern Caspian Region*, Geophys. J. Int. *133*, 630–648.

MCNAMARA, D., OWENS, T., and WALTER, W. (1996), *Propagation Characteristics of Lg across the Tibetan Plateau*, Bull. Seismol. Soc. Am. *86*, 457–469.

MELLORS, R., (1997), *Preliminary Noise Survey and Data Report of Saudi Arabian Data*, *UCRL-ID-128949*, 15pp., Lawrence Livermore National Laboratory, Livermore CA.

MELLORS, R., VERNON, F., CAMP, V., AL-AMRI, A., and GHALIB, A. (1999), *Regional Waveform Propagation in the Saudi Arabian Peninsula* (in press).

MITCHELL, B. J. (1995), *Anelastic Structure and Evolution of the Continental Crust and Upper Mantle from Seismic Surface Wave Attenuation*, Rev. Geophys. *33*, 441–462.

NI, J., and BARAZANGI, M. (1983), *High frequency Seismic Wave Propagation Beneath the Indian Shield, Himalayan Arc, Tibetan Plateau and Surrounding Regions: High Uppermost Mantle Velocities and Efficient Propagation Beneath Tibet*, Geophys. J. R. Astr. Soc. *72*, 665–689.

OLIVER, J., and EWING, M. (1957), *Higher Mode Surface Waves and their Bearing on the Earth's Mantle*, *Bull. Seismol. Soc. Am. 47*, 187–204.

PRESS, F., and EWING, M. (1952), *Two Slow Surface Waves across North America*, Bull. Seism. Soc. Am. *42*, 219–228.

RODGERS, A., NI, J., and HEARN, T. (1997), *Propagation Characteristics of Short-period Sn and Lg in the Middle East*, *87*, 396–413.

RUZAIKIN, A., NERSESOV, I., KHALTURIN, V., and MOLNAR, P. (1977), *Propagation of Lg and Lateral Variations in Crustal Structure in Asia*, J. Geophys. Res. *82*, 307–316.

SEBER, D., BARAZANGI, M., TADILI, B., RAMDANI, M., IBENBRAHIM, A., BEN SARI, D., and OTMAN EL ALAMI, S. (1993), *Sn to Sg Conversion and Focusing along the Atlantic Margin, Morocco: Implications for Earthquake Hazard Evaluation*, Geophys. Res. Lett. *20*, 1503–1506.

SEBER, D., BARAZANGI, M., TADILI, B., RAMDANI, M., IBENBRAHIM, A., and BEN SARI, D. (1996) *Three-dimensional Upper Mantle Structure Beneath the Intraplate Atlas and Interplate Rif Mountains of Morocco*, J. Geophys. Res. *101*, 3125–3138.

SEBER, D., and MITCHELL, B. (1992), *Attenuation of Surface Waves across the Arabian Peninsula*, Tectonics *204*, 137–150.

SHAPIRO, N., BETHOUX, N., CAMPILLO, M., PAUL, A. (1996) *Regional Seismic Phases across the Ligrian Sea: Lg Blockage and Oceanic Propagation*, Phys. Earth Planet. Interiors *93*, 257–268.

VERNON, F., MELLORS, R., BERGER, J., AL-AMRI, A., and ZOLLWEG, J. (1996), Initial results from the deployment of broadband seismometers in the Saudi Arabian shield. In *Proc. 18th Annual Seism. Res.*

Symp. on Monitoring a Comprehensive Test Ban Treaty 4–6 September, 1996, (J. F. Lewkowicz, J. M. MacPhetres and D. T. Reiter, eds.), pp. 108–117.

WALTER, W. R., MAYEDA, K. M., and PATTON, H. (1995), *Phase and Spectral Ratio Discrimination between NTS Earthquakes and Explosions. Part I: Empirical Observations*, Bull. Seismol. Soc. Am. *85*, 1050–1067.

WESSEL, P., and SMITH, W. (1991), *Free Software Helps Display Data*, EOS *72*, 445–446.

XIE, J., and MITCHELL, B. (1990), *A Back-projection Method for Imaging Large-scale Lateral Variations of Lg Coda Q with Application to Continental Africa*, Geophys. J. Int. *100*, 161–11.

ZHANG, T., and LAY, T. (1995), *Why the Lg Phase does not Traverse Oceanic Crust*, Bull. Seismol. Soc. Am. *85*, 1665–1678.

(Received July 14, 1999, revised March 7, 2000, accepted March 10, 2000)